

Contents lists available at ScienceDirect

Physica A: Statistical Mechanics and its Applications

journal homepage: www.elsevier.com/locate/physa





Unbalanced force emanating from stored elastic energy in granular packing: Fundamental insight from quasi-static DEM simulation

Prashant Kumar Jha^a, Shantanu Khawas^b, Debadrita Das^c, Raghavan Ranganathan^d, Kisor Kumar Sahu^{a,*}

- ^a School of Minerals, Metallurgical and Materials Engineering, Indian Institute of Technology Bhubaneswar, Argul, Jatni, Khurda, Odisha 752050, India
- b Department of Metallurgical and Materials Engineering, National Institute of Technology, Rourkela, Odisha 769008, India
- ^c School of Infrastructure, Indian Institute of Technology Bhubaneswar, Argul, Jatni, Khurda, Odisha 752050, India
- d Department of Materials Engineering, Indian Institute of Technology Gandhinagar, Palaj, Gandhinagar, Gujarat 382055, India

ARTICLE INFO

Keywords: Discrete element modelling Granular material Unbalanced force Wall friction test, Iron ore Quasi-static

ABSTRACT

Unbalanced force is poorly understood in discrete simulation of granular packing. During simulation of 'wall friction test' of granular iron ore, sharp peaks of unbalanced force were observed even during a quasi-static condition, contrary to the expected behavior. Particles having maximum unbalanced force were identified and the dynamic behavior of the particle and its neighborhood was thoroughly investigated (no explicit long range force was present in the simulation). It is inferred that the peaks occur due to storage of elastic energy within particles, followed by a sudden/gradual release. Finding of this article might have far reaching consequences in many disparate and diverse disciplines, such as Shear Transformation Zones (STZs) in metallic glasses, identifying tiny but non-trivial configurational changes at the onset of glass transition as well as for its relaxation behavior, origination of specific structural features (say, origin of stacking faults) in High Entropy Alloys (HEAs), kinetic instability induced symmetry breaking in granular media, Self-Organized Criticality (SOC) induced avalanching in granular systems etc. The unbalanced force index can turn out to be a very important metric for analyzing the configurational instability of those particulate ensemble for quasi-static and static conditions.

1. Introduction

Granular materials are used in a wide range of industrial applications such as in food processing, powder metallurgy, pharmaceuticals, semiconductor, mining etc. [1–3]. The static and flow properties of granular packing govern their efficacy and performance, and hence, it becomes very important to understand them at a fundamental level. Generally, physics-informed replication and simulation of real-life granular assemblies is performed through the Discrete Element Method (DEM) [4]. It is a numerical protocol for simulating the forces between individual discrete particles, therefore well-suited for studying the collective dynamics of a packing consisting of a large number of particles. Different theories have been developed to model the granular flow accurately. Duan et al. [5]

E-mail address: kisorsahu@iitbbs.ac.in (K.K. Sahu).

https://doi.org/10.1016/j.physa.2025.130604

^{*} Corresponding author.

proposed that, granular shear flow occurs in inertial regime, elastic regime and transition regime; so the consideration of elastic potential energy of the system is extremely important. They also emphasized the importance of including the particle stiffness in modeling granular flow to account for elastic potential energy during inter-particle collisions. This is in contrast to the kinetic theory which assumes no dissipation of elastic potential energy caused by deformation due to particle collisions. The resulting Soft-Sphere Kinetic Theory (SSKT) model takes particle stiffness as input and models its effect on transfer between kinetic energy and elastic potential energy of the particles, including the change in kinetic energy that occurs due to elastic potential energy. The transfer between kinetic energy and elastic potential energy has also been studied [5] where they have elucidated inelastic particle-particle and particle-wall collisions and the subsequent transition of kinetic and gravitational potential energy into elastic potential energy.

The complete energy balance equation for particle-particle collisions can be captured by the following relation: [6]

$$\delta W = \delta \psi_{e} + \delta \phi_{n} + \delta \phi_{s} + \delta \phi_{redist} \tag{1}$$

where, δW , $\delta \psi_e$, $\delta \phi_p$, $\delta \phi_s$ and $\delta \phi_{redist}$ represent change in external work, elastic energy, plastic dissipation energy, breakage energy and redistribution energy, respectively. The elastic energy for a given particle i is the summation over all its contacts, given as:

$$\psi_e^i = \Sigma \frac{8}{15} E^* \sqrt{R^*} \quad d^{\frac{5}{2}} \tag{2}$$

where, d is the inter-particle overlap, E^* and R^* are the effective Young's Modulus and radius of particles in contact [7]. In this study, we have used the open source DEM particle simulation software LIGGGHTS^(R) [8] (which is essentially adapted from the molecular dynamics package, LAMMPS [9] and improved for general granular and granular heat transfer simulations).

For industrial applications of granular packing, wall friction test is frequently performed to investigate the particle-wall interaction properties such as coefficient of static and rolling friction [10]. For optimal design of storage or handling equipment (e.g. silos, chutes etc.), it is important to study the flow of bulk solids across their surface and ensure appropriate flow patterns inside them. The flow patterns are primarily governed by kinematic wall friction [10]. It is defined as the ratio of normal stress to constant shear stress. As normal stress is applied on a granular assembly, it undergoes deformation resulting in the increase of elastic deformation energy [11]. An important quantity that characterizes the imbalance in forces during the granular flow is the unbalanced force index (I_{uf}), defined as the ratio of resultant force to the contact force of the particles in the simulation [12]. Granular systems are sensitive to input parameters, in order to choose the appropriate value of the parameters, mostly calibration is done with certain known behavior of granular materials. To perform any sensitivity analysis of the input parameters, it is a good practice to keep the unbalanced forces for the simulations below a certain limit to ensure equilibrium. In the article by Ng [12], the unbalanced force is keep thelow 0.01, since the effect of all input parameters used in the study are negligible. Similarly, Foroutan et al. [13] also kept unbalanced force value below 0.01 so that the system can be considered quasi-static in nature. We also followed the similar practices in this article. During the wall friction simulation of a granular sample (iron ore) using DEM software LIGGGHTS^(R), we observed abnormalities in the unbalanced force index (UBF index). The average UBF index is calculated as given in (Eq. (3)):

$$I_{uf} = \sqrt{\frac{\frac{1}{N_p} \sum_{p=1}^{N_p} (f_{res}^p)^2}{\frac{1}{N_c} \sum_{c=1}^{N_c} (f^c)^2}}$$
(3)

where, N_c and N_p are the total number of contacts and particles respectively, f_{res}^p is the resultant force and f^c is the contact force on each particle. The present work reports peaks of I_{uf} greater than 0.01 at various time-steps during quasi-static loading. We hypothesize that this phenomenon occurs when some particles of the packing experience sudden change in velocity due to the release of stored elastic energy. Through a detailed tracking of granular particles, the ones having highest unbalanced force are identified, and their

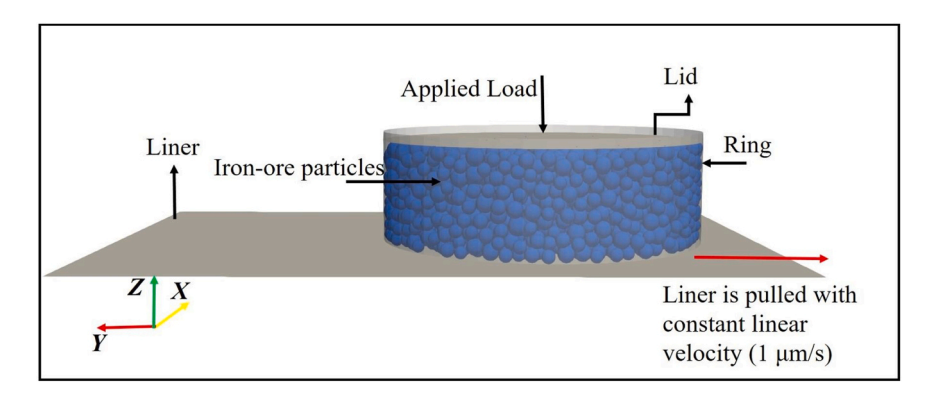


Fig. 1. Represent schematic of wall friction test setup where a constant normal force is applied on lid and liner is pulled in negative Y direction with a constant velocity (1.0 μ m/s) due to which shearing of granular material (iron-ore) takes place. The radius of the ring is 0.45 m and height till which particles are filled is 0.27 m.

displacements, velocities, contact force, resultant force and elastic and kinetic energy are tracked to derive a holistic understanding of the phenomena.

2. Method

2.1. Theory

The standard test procedure to study particle-wall interaction (wall friction test) is based on the Jenike Shear Tester [14] which consists of a shear cell as schematically shown in Fig. 1. The shear cell typically consists of a liner (whose surface properties are to be evaluated), a ring upon the liner (for confining the material) and a lid (to avoid overflow and/or to exert additional normal force). The ring is completely filled with the granular material and a vertical normal force is applied on the lid to consolidate it. In order to measure the kinematic wall friction, the ring or the liner is driven with a constant velocity.

2.2. Simulation details

For the present study, a wall friction test simulation was performed in LIGGGHTS^(R) using an iron ore sample with 2712 granular particles. The particle-size distribution is given in the supplementary (Fig. S1). The material properties of the iron ore are shown in Table 1 and the interaction properties used in the simulation are shown in Table 2.

During wall friction simulation, the wall shear stress increases with time. Eventually a steady state of wall shear stress is attained, which is unique for a given normal stress (refer to supplementary S2 for details). The wall friction simulation is performed for a range of normal force, ranging from 1 to 2.5 kN, corresponding to unique values of steady state shear stress. The ratio of steady state shear stress (τ_w) to normal stress (σ_w) gives the coefficient of kinematic wall friction (μ) (Eq. (4)). For this study, normal load of 2 kN is applied to attain a steady state shear stress condition.

$$\mu = \frac{\tau_w}{\sigma} \tag{4}$$

In Table 2, the values depicted in column 2 (for very dry iron-ore; 5 % moisture content) and column 3 (for very wet iron-ore; 14.5 % moisture content) were obtained through a newly developed calibration protocol [16]. The coefficient of restitution assigned to the particles in this study is 0.15 and obtained from literature [17]. The very dry iron-ore represents the best class of iron-ore as far as the flow properties are concerned, while the very wet iron-ore represents the worst class of iron-ore. It is worth noting here that moisture content of more than 15 % in the iron-ore represents a supersaturated condition and therefore, their flow properties are fluid-like and not amenable to DEM studies. The particle-particle interaction values used for this article is chosen in consultation with the concerned iron-ore industry (NMDC Ltd., India [18]) and represent a somewhat intermediate grade of iron-ore from the material flow perspective. Since this study aims to capture the intrinsic nature of the material under study (intermediate grade iron-ore) and not a heterogeneous liner-material interaction, therefore, we deliberately chose the particle-wall interaction values to be exactly the same as particle-particle interaction values. This is essentially equivalent to capturing the flow properties of iron-ore onto a liner consisting of iron-ore itself (for capturing flow properties deep inside the bulk flow regime). The simulation consists of four stages. The first stage (Fig. 2(a)) involves particle insertion for filling up the cylindrical ring, followed by the second stage (Fig. 2(b)) of deleting excess particles generated outside the system (ring). The third stage (Fig. 2(c)) is the preconsolidation stage where a normal force of 2 kN is applied on the lid. Following this, in the fourth stage (Fig. 2(d)) the liner is pulled in the negative y direction at a constant velocity of 1.0 µm/s to maintain a quasi-static state. The velocity was deliberately kept very low in order to achieve quasi-static conditions easily. Fig. 2(e) represents the variation of average UBF index for all the particles as a function of time. Large unbalanced force can be seen at the time step when the liner starts to move (2.5 s), but as the system approaches quasi-static state the unbalanced force drops down to a steady value (approximately to zero). But after 2.8 s, sudden peaks in the unbalanced force were observed. This indicates that the system changes its state from quasi-static to a somewhat non quasi-static state despite the absence of any other external force apart from the constant liner velocity. Therefore, the analysis of the peaks is done from 2.8 s onwards. For the sake of brevity this article only analyzed all the three peaks having UBF index greater than 0.01. Analysis of the other minor peaks will be published elsewhere.

Hertz-Mindlin contact models [19] were used for normal and tangential contacts forces (F_n and F_t) respectively and were evaluated using Eqs. (5) and (6). The normal and tangential damping coefficients (γ_n and γ_t), were evaluated using the Eqs. (7) and (8) respectively.

$$F_{n} = \frac{4}{3}E^{*} \sqrt{R^{*}} d_{n}^{3/2} - \gamma_{n}V_{rel}^{n}$$
 (5)

Material properties used in the simulation.

Parameter	Value
Iron-ore particle density (kg/m³) Young's Modulus of iron-ore [15] (MPa) Poisson's ratio of iron ore [15]	2700 40 0.25

 Table 2

 Parameters used for particle-particle interaction in the simulation.

Parameter	Calibrated value for very dry iron-ore (5 % moisture content) [16]	Calibrated value for very wet iron-ore (14.5 % moisture content) [16]	Value used for this study
Coefficient of static friction	0.6	0.97	0.85
Coefficient of rolling friction	0.2	0.58	0.40

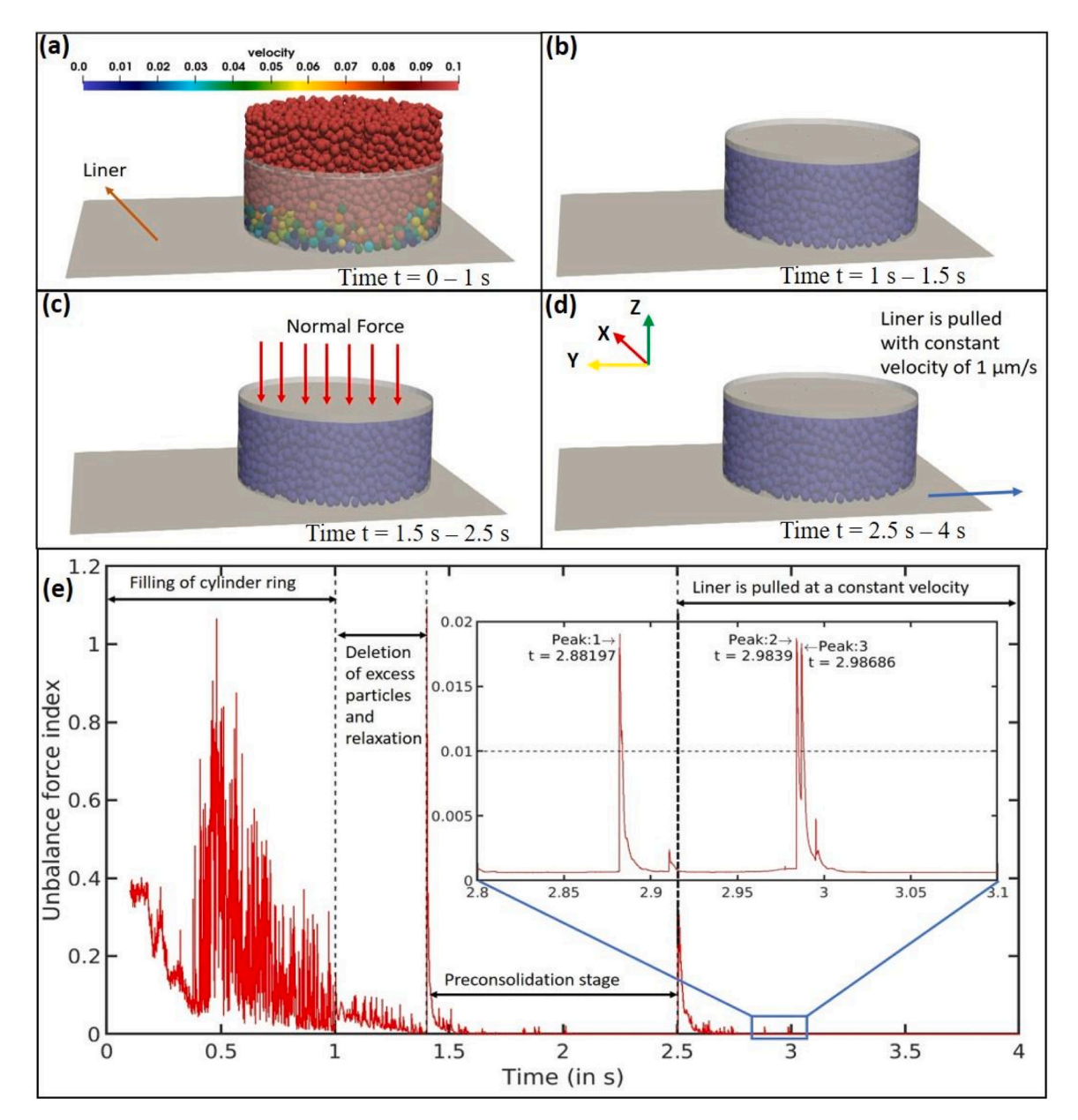


Fig. 2. Replication of wall friction test used in the simulation, (a): Ring is filled with particles, (b) Deletion of the excess particles beyond the ring brim, (c) Normal force is being applied on the lid, (d) Liner is being pulled with constant velocity, (e) Variation of unbalanced force from the start of the simulation to the end of simulation (three different peaks have been identified at different time intervals and sequentially named as peak 1, 2 and 3 depicted in the inset of (e)).

$$F_t = 8G^* \sqrt{R^* d_n} d_t - \gamma_t v_{rel}^t$$

$$\tag{6}$$

$$\gamma_n = -2\sqrt{\frac{5}{6}} \frac{\ln e}{\sqrt{\ln^2 e + \pi^2}} \sqrt{2E^* l\sqrt{R^* d_n} m^*}$$
(7)

$$\gamma_t = -2\sqrt{\frac{5}{6}} \frac{\ln e}{\sqrt{\ln^2 e + \pi^2}} \sqrt{8E^* \sqrt{R^* d_t} m^*}$$
 (8)

The Coulomb friction criterion is implemented for the tangential force (Eq. (9)):

$$|F_t| \le \mu_s |F_n| \tag{9}$$

here, v_{rel}^n and v_{rel}^t are the normal and the tangential components of the relative velocity of the two particles respectively, e is the coefficient of restitution, μ_s is the coefficient of static friction, d_n is the normal overlap, d_t is the tangential overlap and m^* , R^* , E^* , G^* , are mass, radius, Young's modulus and shear modulus of two particles in contact respectively, where * in the suffix represents an effective parameter.

Practically all the real particles are irregular in shape hence to account for irregular shape of the actual particles in this study, additional rolling friction is applied. Rolling contact model [20] (Eq. (10)) is added that corrects the motion by transferring additional moment (T_{ri} , r, n in the subscript stands for rolling and normal).

$$T_r = \mu_r F_n d_n \frac{W_{r,shear}}{|W_{r,shear}|R^*}$$
(10)

where, $w_{r,shear}$ is the projection of the relative angular velocity w_r into the shear plane, μ_r is the coefficient of rolling friction.

The coefficient of static friction and the coefficient of rolling friction were assigned for particle-liner and particle-particle interaction as shown in Table 2. However, no values were assigned to particle-ring and liner-ring interactions, which eliminates the need to consider properties of the ring (assuming a frictionless ring).

3. Sensitivity analysis

In DEM simulations, it is important to use time step (Δt) equals to 20 % of the Rayleigh time (Δt_r) [21] to ensure numerical stability. The formula for calculating the Rayleigh time is given below.

$$\Delta t_{\rm r} = \frac{\pi R_{\rm min}}{C_R} \tag{11}$$

where, $C_R = \frac{0.862 + 1.14\nu}{1 + \nu} \sqrt{\frac{E}{\rho}}$

 $R_{\min} = \min \max \text{ radius of the particle}$

 $\nu = \text{Poisson's ratio of the particle}$

E =Young's modulus of the particle

 $\rho = \text{solid}$ density of the particle

For the sample used in this study, Δt turns out to be 1.5×10^{-4} s. However, to maintain a quasi-static system, we have chosen a Δt to 10^{-6} , which is nearly 100 times smaller than the Rayleigh time. To further assess the impact of numerical stability in the simulation, we repeated the simulations using different Δt values: 10^{-5} , 10^{-6} and 10^{-7} s in Fig. 3. The Δt values 10^{-7} and 10^{-6} s give almost similar trend in the UBF index, but for Δt values 10^{-7} s require significantly more computational time. Therefore, we selected 10^{-6} as the optimal Δt value for our study.

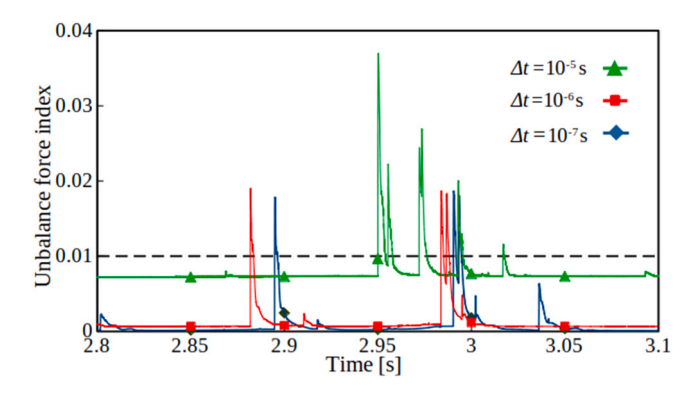


Fig. 3. Effect of time step (ranging from 10^{-5} to 10^{-7} s) on to UBF index peak.

The sensitivity analysis of UBF index concerning variations in contact parameters, including particle-particle ($\mu_{s(pp)}, \mu_{r(pp)}, k_{(pp)}, e_{(pp)}$) is shown in Figs. 4(a–j) and 5(a–j) and for particle-liner ($\mu_{s(pl)}, \mu_{r(pl)}, k_{(pl)}, e_{(pl)}$) is provided in supplementary S3 (NOTE: μ , k, e denotes coefficient of frictional force, cohesion energy density and coefficient of restitution; s and r in suffix denote static and rolling parameters; pp and pl within parenthesis denote particle-particle and particle-liner properties, respectively). To assess the sensitivity of the UBF index, we have selected values on either side of our calibrated parameter. For instance, to study the sensitivity of the parameter $\mu_{s(pp)} = 0.85$, we consider two lower values (0.75, 0.8) and two higher values (0.9, 0.95). Note that the parameters that have been used in this study are identified by a green box around the plots in Figs. 4(c, h) and 5(a, h). This approach ensures a thorough evaluation of the impact of these variations. It is found that the UBF index peaks height do not have a significant effect whereas position of occurrence of peak changes.

Special attention need to be given to the cohesion energy density (k) values, which we set to zero (Fig. 5(a)). Even when cohesion energy density is considered, peaks in unbalanced forces still appear, though their values vary within the range of 10^2-10^5 J/m³. This indicates that while cohesion may influence the system's behavior, it does not entirely eliminate fluctuations in unbalanced forces. Therefore, to simplify the interpretation of the simulations results, we set k to zero, as we wanted to bypass the complexities arising from the consideration of k.

4. Results and discussion

The calculated average UBF index of all the particles at different time steps were plotted as a function of time as shown in Fig. 2(e). It reveals that in spite of the system being in a quasi-static state during the time interval of 2.8 - 3.1 s, three major peaks (> 0.01) in unbalanced force index were observed (inset of Fig. 2(e)) at 2.88197 s, 2.98390 s and 2.98686 s and will be referred to as peak 1, 2 and 3 respectively. The particle having the highest unbalanced force on an average for the entire duration of a peak is termed as a 'prime' particle. It is expected that a close investigation of the time evolution of the immediate neighborhood (cut-off distance defined as 1.1* $(r_{prime}+r_{maximum}))$ of the prime particle might reveal very useful insights. Here, r_{prime} and $r_{maximum}$ are the radius of a prime particle and the maximum radius (25 mm) of a particle in the system respectively. In order to justify the cut-off distance, Radial Distribution Function (RDF) of the sample is plotted (supplementary \$4.1) to analyze the local structure/environment. The first peak in the RDF indicates the nearest neighbor distance, representing the most probable separation between a reference particle and its closest neighbors. To determine the neighborhood of the "prime" particle, the cutoff distance is chosen near the end of the first peak, as this marks the maximum extent of the nearest neighbor shell. The rationale for this expectation stems from the absence of long range attractive forces between the particles owing to their granular nature and the repulsive force directly interacting with the first neighbors alone. The particles present in this neighborhood of prime particles are named as 'neighbor' particles. The location of these three clusters (at the instant of their respective peak in UBF index) are depicted in Fig. 6(a). The position of the prime particle and their distance (d_p) from the confining ring is shown in the inset table in Fig. 6(a). Fig. 6(b) shows the average overlap of all the particles for all the time in the system. In the first stage (0-1 s) is the filling of the ring with particles, therefore there is lots of fluctuation in overlap.

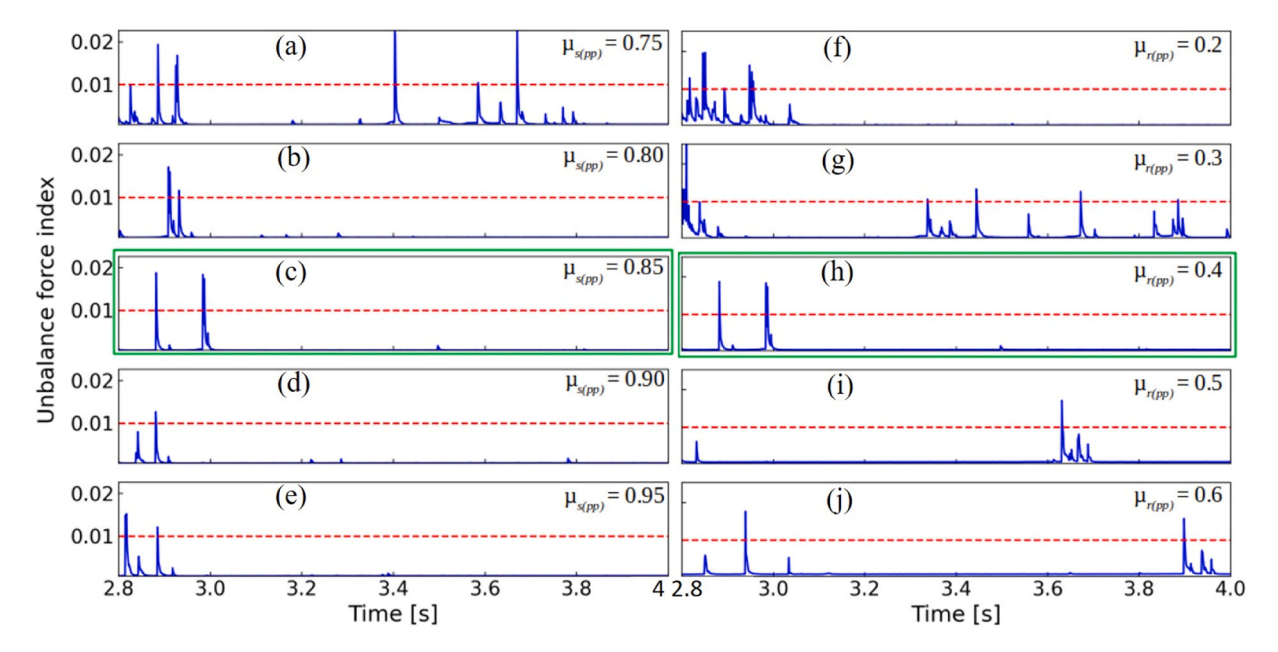


Fig. 4. (a–e) Effect of coefficient of static friction between particle-particle ($\mu_{s(pp)}$) ranging from 0.75 – 0.95 on to the UBF index. (f–j) Effect of coefficient of rolling friction between particle-particle ($\mu_{r(pp)}$) ranging from 0.2 to 0.6 on to the UBF index. Note that $\mu_{s(pp)}$ and $\mu_{r(pp)}$ used in our article is 0.85 and 0.4 respectively (highlighted by the green box in center). Horizontal red dashed line represent UBF threshold of 0.01 (refer the discussion of Eq. (3)).

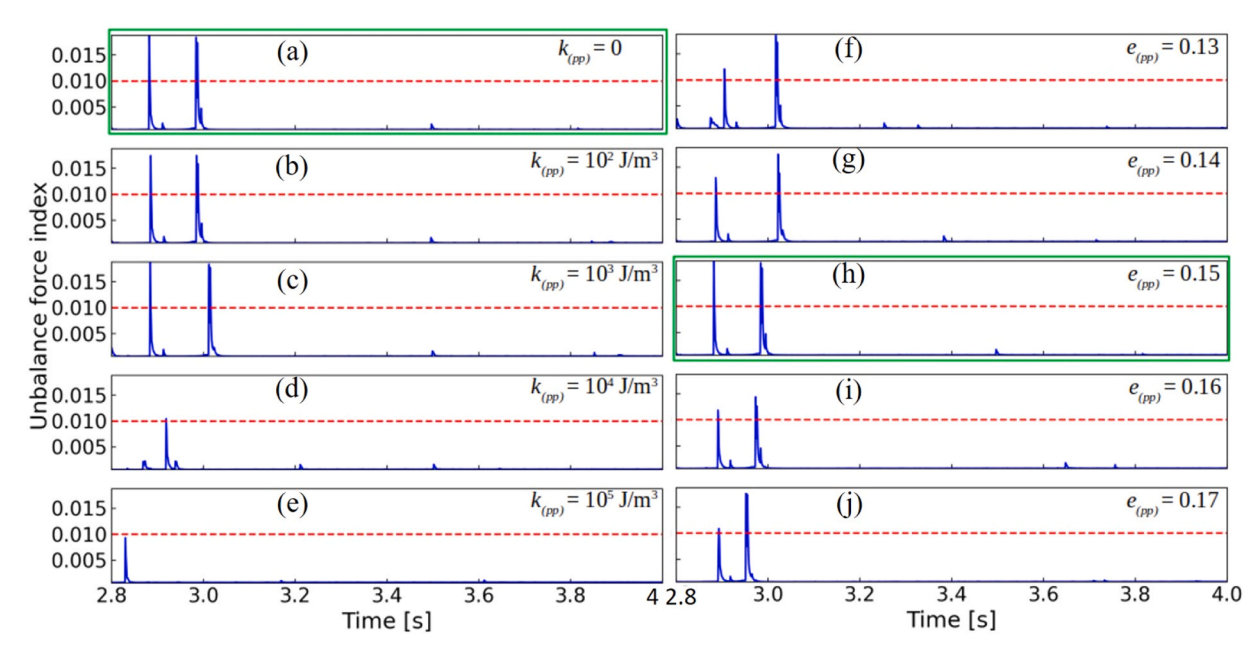


Fig. 5. (a–e) Effect of cohesion energy density between particle-particle $(k_{(pp)})$ ranging from 0 to 10^5 J/m³ on to the UBF index (f–j) Effect of coefficient restitution between particle-particle $(e_{(pp)})$ ranging from 0.13 to 0.17 on to the UBF index. Note that $k_{(pp)}$ and $e_{(pp)}$ used in our article is 0 and 0.15 respectively (highlighted by the green box). Horizontal red dashed line represent UBF threshold of 0.01 (refer the discussion of Eq. (3)).

In the second stage (1-1.5~s) is the deletion of excess particles, therefore, a slight decrease in the average overlap can be seen. In the third stage (1.5-2.5~s) is the preconsolidation stage, where normal force is applied to preconsolidate the particle, therefore a slight increase in average overlap can be seen. In the fourth stage (2.5~o) nwards) the liner is pulled at a constant velocity of $1~\mu$ m/s, thus the average overlap remains constant thereafter. But it is to be noted that as we start to pull the liner at 2.5~s, there is slight decrease in the average overlap due to the fact the servo wall (which exerts normal force on the particles) slightly adjust its position. And we also indicated the three peaks in red triangles to show that there is no anomaly in the average overlap parameter at the three peak locations. The total overlap for the particles in cluster at peak 1~s is shown in supplementary Fig. S4.2. Fig. 6(c) depicts the velocity of all the particles in the system during the entire quasi-static state of interest (time = 2.8~s to 3.01~s) spanning all the three peaks. For clarity, the velocities of three prime particles are highlighted by markers and clearly they show remarkably distinct behavior than other particles which are well correlated with the peaks in UBF index. The analysis of this anomalous dynamical pattern (note that the entire system is held in a place by the ring and only the liner is moving) is the prime theme of this article.

The data for the displacement of the prime and neighbor particles were calculated as follows (will be clearly distinguished when results are presented):

- a. With respect to the position of the particles at time 2.8 s (reference point near peak 1 having low UBF index).
- b. With respect to the position of the particles at the start of the peak (2.88 s for the first peak; Table 3).

The start and end time-steps of the peaks, the prime and neighboring particle IDs and prime particles radius are mentioned in Table 3.

The UBF index plot (Fig. 7) for the particle cluster of peak 1 depicts that the prime particle has a maximum UBF index of approximately 20 at around 2.89 s. The vertical red dotted line (with two red triangles at both ends) in all the subsequent figures (Fig. 7 onwards) represent the position of the peak being analyzed. The other neighboring particles have significantly lower UBF index as shown in the inset in Fig. 7(a). The contact and resultant forces of the prime and its neighbors are depicted in Fig. 8. It can be seen that there is a sudden increase in contact force and resultant force on the prime particle. However, it should be noted here that particle ID 1135, 1140 and 1280 also experience a sudden change in contact force at the time-step of the peak but the other neighboring particles with IDs 1263 and 1273 do not show much change. The particles showing the sudden change in contact force have a positive overlap (when two particles are in contact) and the others have a negative overlap (two particles not in contact) with the prime particle referred to in the supplementary (Fig. S4.3).

To investigate further the cause of high unbalanced force of the prime particle, the displacement and velocity of prime and neighboring particles were plotted for the time-interval of peak 1 (2.88–2.9 s) and for the time of the interest (2.8–3.01 s; during the quasi-steady state). Fig. 9 depicts the displacement of the cluster in x, y and z-direction with respect to their positions at time 2.8 s, involving the prime particle 1264 and its neighbors. The displacement of the prime particle increases drastically from 2.8 s but it remains constant after the attainment of the peak. It is important to note here that the entire system is kept stationary and the liner is externally driven in negative y direction with a velocity of 1.0 μ m/s. It is interesting to see that the displacement of the prime particle

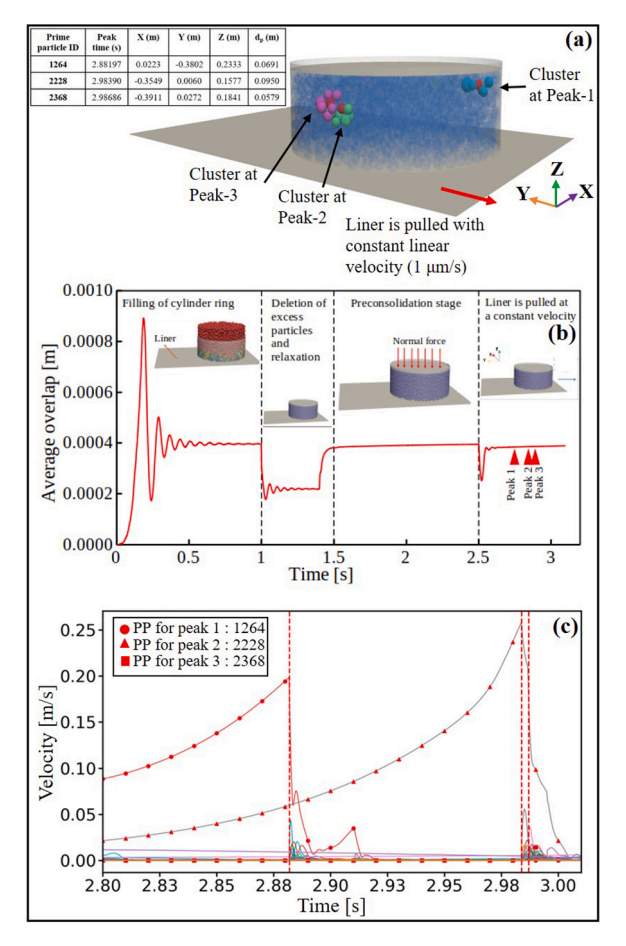


Fig. 6. (a) Represent the location of the three clusters in the assembly of particles, where the red color depicts the prime particle in all the clusters. Blue, green and magenta represent the neighbor particles at peak 1, 2 and 3 respectively. Table on the top-left corner represents the position of the prime particle in 3D space at their peak time and distance of prime particle from ring is denoted as d_p (b) Represents the average overlap of all the particles for all the time in the system from start of the simulation to 3.1 s (c) Represents the variation of velocity of all the 2712 particles in the system during the time interval of interest (from 2.8 to 3.01 s; since low UBF index observed at 2.8 s and 3.01 s). The prime particles for all the three peaks are identified by additional markers. The PP denotes prime particle.

Table 3Time-step and particle ID of the respective peaks.

Peaks	Starting time (s)	Ending time (s)	Prime particle ID	Prime particle radius (in m)	Neighbor particles' ID
Peak 1	2.88000	2.90000	1264	0.017	1135, 1140, 1263,1273,1280
Peak 2	2.98000	2.98658	2228	0.018	848, 849, 975, 1971, 2107, 2108
Peak 3	2.98658	3.01000	2368	0.017	986, 2094, 2107, 2240, 2369, 2379, 2483

begins to rise from 2.8 s itself, however the UBF index occurs much later, around 2.89 s. This could be because the prime particle shoots out in the beginning but later displacement becomes similar to its neighboring particles. The central question is: where the prime particle gets the energy for this unusual rate of displacement? Under ideal conditions, when there is no friction between the particle and the liner, the particle should not have any relative displacement and velocity with respect to the liner, since the liner is pulled with constant velocity (and the confining ring is kept stationary). Any displacement or velocity of the particles can be attributed to presence of friction among the particles and the liner. It should be noted that the liner velocity ($1 \mu m/s$), which is the only source of externally applied force to the system, is insignificant compared to the prime particle displacement (and also the velocity as discussed later). Therefore, the only plausible cause of this unusual movement of the prime particle can be attributed to the stored elastic energy.

Fig. 10 shows the displacement of only the neighboring particles from time-step 2.8 s, (since the displacement of the neighboring particles is way lower than the prime particle, the data for the prime particle has been omitted for clarity). Particle IDs 1140 and 1135 show anomalous displacement patterns (in the direction of liner movement in negative y direction but at a much faster velocity than the liner velocity of 1 μ m/s; Fig. 10(b)) with respect to displacement of the liner. Now let us focus on the close vicinity of peak 1, i.e.

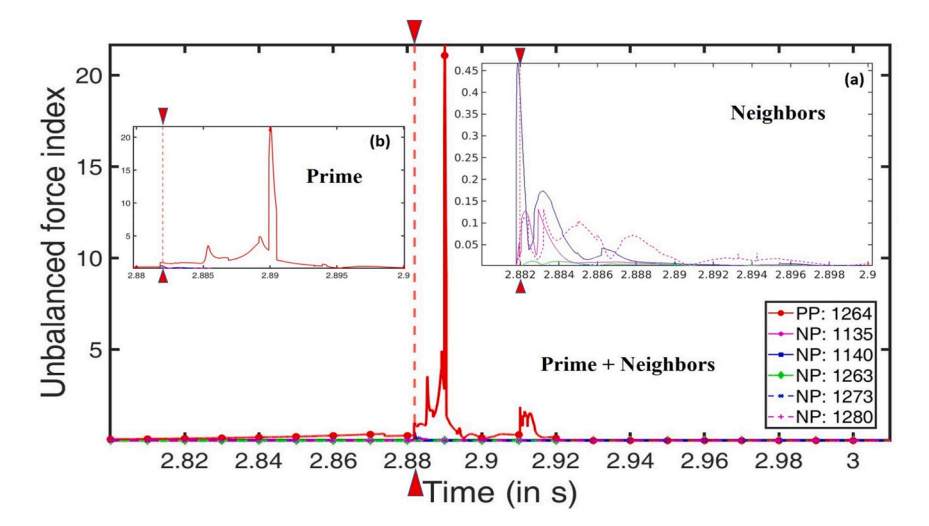


Fig. 7. Collective UBF index plot of peak 1 for prime and neighbor particles only, inset (a) UBF index for neighbor particles alone and inset (b) UBF index for prime particle only. Notation in the legend: PP refers to the prime particle and NP refers to the neighbor particles.

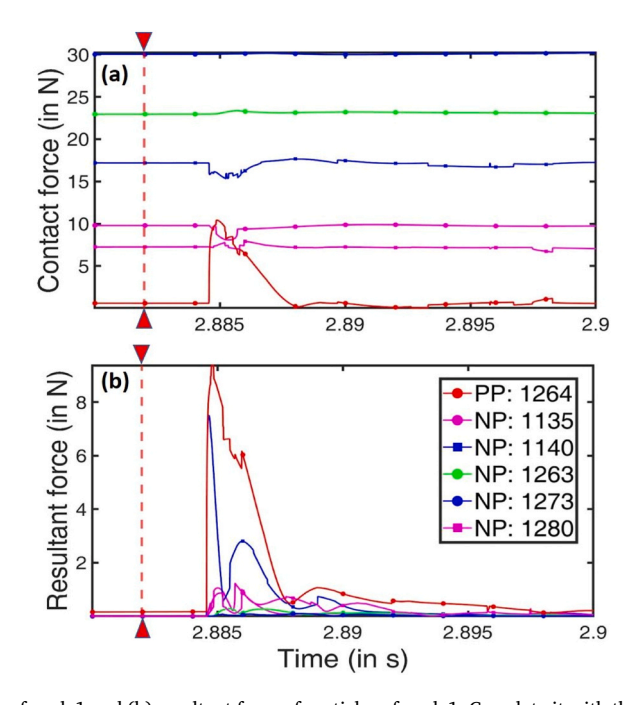


Fig. 8. (a) Contact force of particles of peak 1 and (b) resultant force of particles of peak 1. Correlate it with the overlap plot in supplementary S4.3. See text for details.

instead of plotting displacement from 2.8 s (Fig. 9), we will be plotting from the start of the peak, i.e. 2.88 s in Fig. 11 for displacement of prime particle (and displacement of neighbor particles is added in the supplementary Fig. S5.1). From the plots, it is evident that the prime particle has much higher displacement compared to neighboring particles, which indicates that it travels a greater distance at the same time interval.

A similar trend can be seen from the velocity plots (Figs. 12–14), which further corroborates the idea of stored energy release. The velocity of the prime particle is seen to be higher (order of 2) than the neighboring particles and the liner velocity. It is to be noted that the disproportionate change in velocity of the prime particle cannot be explicitly caused by the external driving force alone and most likely arise from the release of stored energy. It is quite reasonable to expect that the particles got deformed elastically in previous steps (since standard DEM implemented in this study does not allow for permanent plastic deformation). When this stored elastic energy was relieved, it caused a sudden change in UBF index which further caused a velocity change far greater than the liner velocity itself. Therefore, it establishes a causality chain.

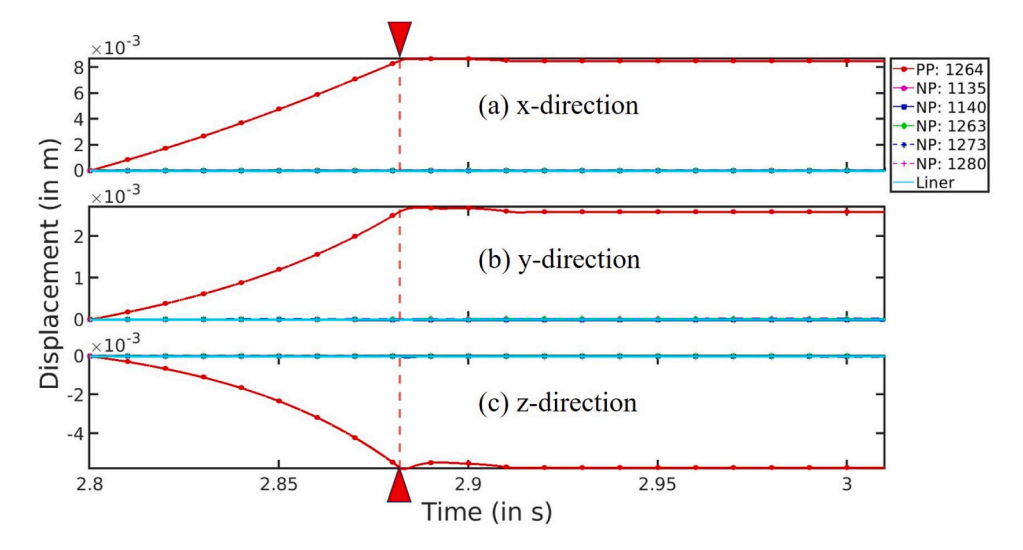


Fig. 9. Displacement in x, y and z-direction for peak 1 from time-step of 2.8 s, where PP means prime particle and NP means neighboring particles.

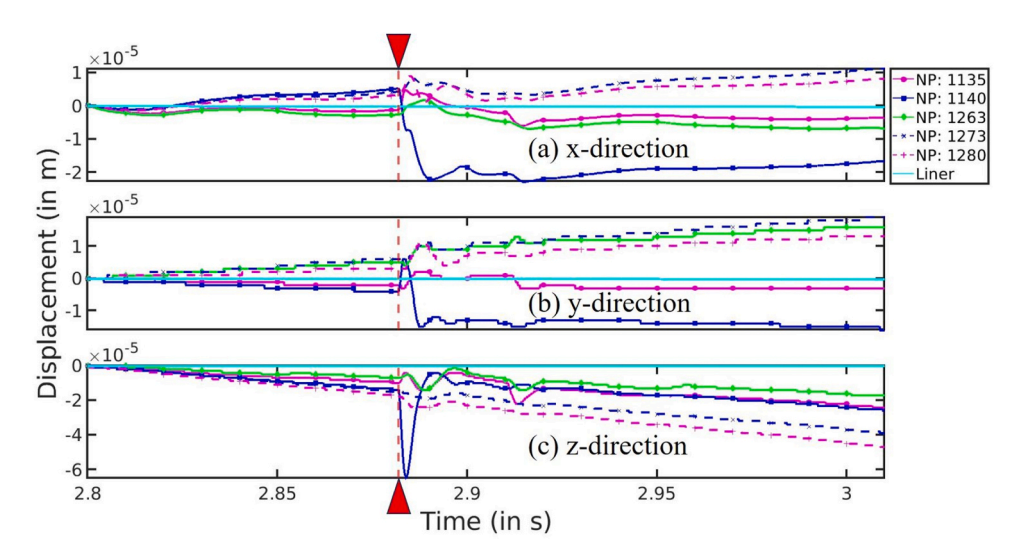


Fig. 10. Displacement in x, y and z-direction for peak 1 from time-step of 2.8 s, excluding the prime particle.

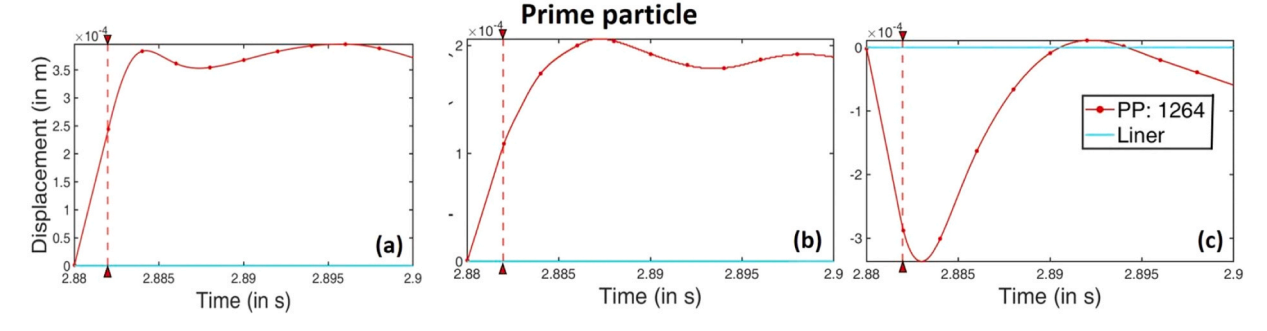


Fig. 11. (a–c) shows the displacement of the prime particle of peak 1 in x, y and z direction respectively, with respect to their coordinates at the start of the peak at time-step 2.88 s.

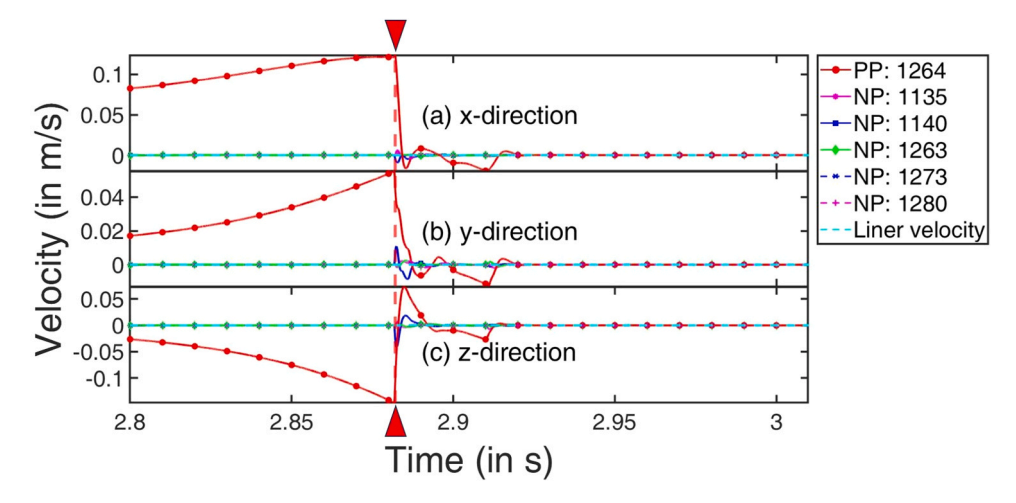


Fig. 12. Velocity in x, y and z-direction for peak 1, from the initial time-step of 2.8 s.

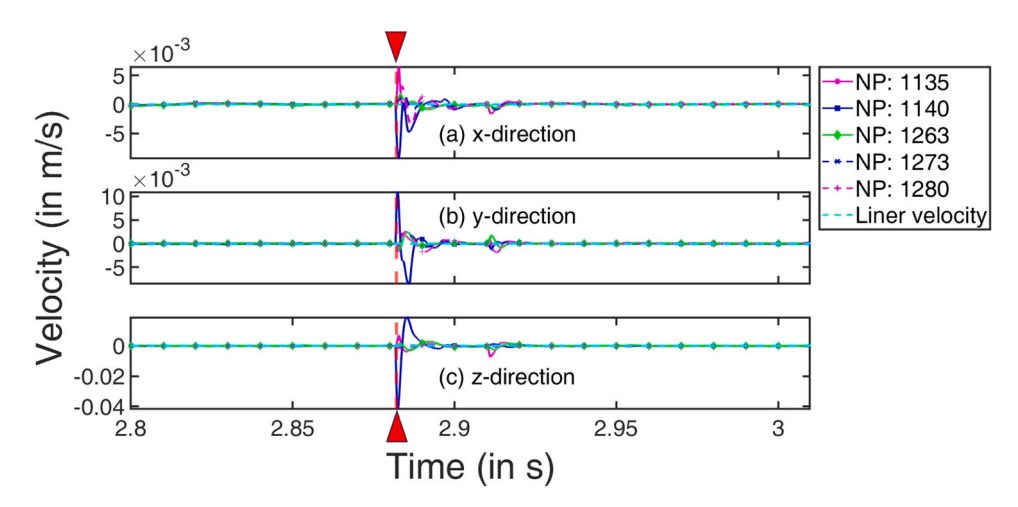


Fig. 13. Velocity in x, y and z-direction for peak 1 (excluding the prime particle) from the initial time-step of 2.8 s.

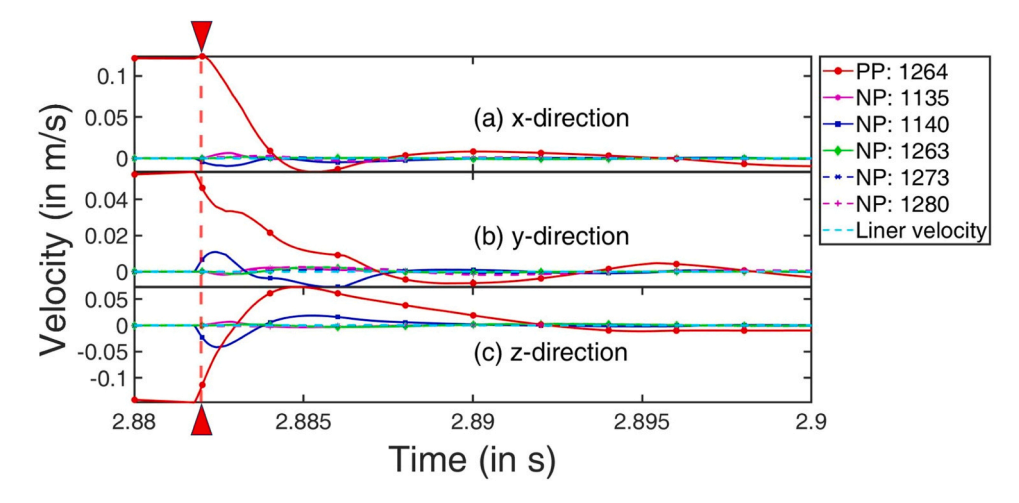


Fig. 14. Velocity of prime and neighboring particles of peak 1 during the occurrence of peak 1 from 2.88 s to 2.9 s.

The elastic energy variation for the particles in cluster at peak 1 from 2.8 to 3.1 s is shown in supplementary S5.2. Fig. 15 provides concrete evidence that there is significant buildup of stored elastic energy (using Eq. (2)) before the appearance of the first peak in the UBF for the prime particle. This is completely consistent with the conjecture/central theme of the present article and provides the strongest proof for our hypothesis.

The analysis of peaks 2 and 3 also support the conjecture of stored elastic energy-driven unbalanced force peaks and are provided in the supplementary document (sections S6 and S7) for the sake of brevity.

5. Authors' perspective

For experimental validation of the displacement, a photo-elastic disk test can be conducted to analyze particle displacement during the wall friction test. This involves using disks of different sizes and tracking their positions and overlaps to determine forces. A similar experimental dataset was generated by Karen et al. [22] where 29 randomly arranged photo-elastic disks of varying sizes were compressed, with the applied external force being transmitted through contact points to the lower discs. But unfortunately that study did not include any analysis of the UBF index, since that was not the theme of that article. However, experiments on similar lines may be conducted in future to experimentally verify the conjecture proposed in this article.

Identifying instability in particulate ensemble is at the core of many important phenomena, such as the Shear Transformation Zones (STZs) in metallic glasses, identifying tiny but non-trivial configurational changes at the onset of glass transition as well as for its relaxation behavior, origination of specific structural features (say, origin of stacking faults) in High Entropy Alloys (HEAs), kinetic instability induced symmetry breaking in granular media [23], Self-Organized Criticality (SOC) induced avalanching in granular systems [24] etc. For example, it is still an open challenge in the glass community to elucidate the reasons for relaxation behavior of small atomic clusters and their displacements during deformation. Although, the role of unbalanced force index into those phenomena is not thoroughly explored to the best of our knowledge, the findings of the present article drop an interesting hint about its suspected role as a common thread behind such diverse and seemingly unconnected phenomena, which warrants a thorough investigation. In that case, the unbalanced force index can turn out to be a very important metric for analyzing the configurational instability of particulate ensemble for quasi-static and static conditions.

6. Conclusion

The wall friction test for iron ore was replicated through simulation and its UBF index was studied. The occurrence of peaks in the unbalanced force plot even after attainment of equilibrium is investigated. The process follows systematic identification of the cluster of particles displaying maximum unbalanced force at that time-step and consequently plotting their contact and resultant force, displacement and velocity. The plots show that the particle with maximum unbalanced force at a time interval deviates in position largely from its neighboring particles, showing a greater magnitude of velocity than the liner. The study depicts that such a phenomenon can only occur due to release of stored elastic energy. The results formulated from this article can be used to understand the behavior of the particles as a cluster. It is very important to study this behavior because the effects of forces of the particles on one another lead to impactful changes in the system, like in our case the UBF index.

Author contributions

All the authors have equally contributed to the work.

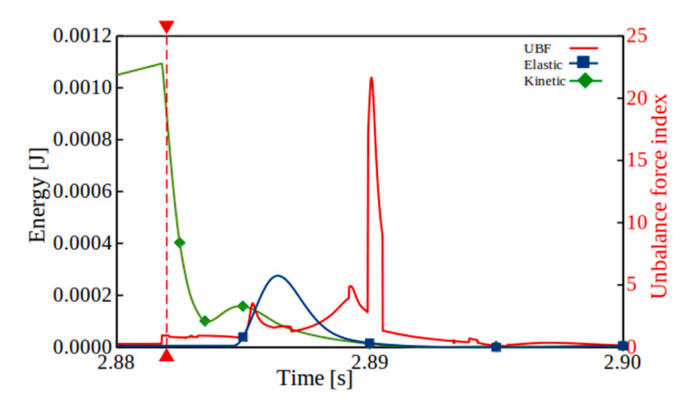


Fig. 15. Elastic, kinetic energy and UBF index variation at the instance of occurrence of peak 1 for the prime particle. UBF index scale has been provided on the right-hand side (secondary y-axis in red color).

CRediT authorship contribution statement

Shantanu Khawas: Writing – review & editing, Writing – original draft, Methodology, Investigation, Formal analysis, Conceptualization. Prashant Kumar Jha: Writing – review & editing, Writing – original draft, Methodology, Investigation, Formal analysis, Conceptualization. Raghavan Ranganathan: Writing – review & editing, Writing – original draft, Supervision, Investigation, Formal analysis. Debadrita Das: Writing – review & editing, Writing – original draft, Methodology, Investigation, Formal analysis, Conceptualization. Kisor Kumar Sahu: Writing – review & editing, Writing – original draft, Supervision, Project administration, Methodology, Investigation, Funding acquisition, Formal analysis, Conceptualization.

Funding

The authors did not receive support from any organization for the submitted work.

Declaration of Competing Interest

The authors declare that they have no known competing financial interests or personal relationships that could have appeared to influence the work reported in this paper.

Acknowledgement

The authors express their sincere gratitude to NMDC Ltd., India, for their invaluable technical support in this research. Special gratitude to S K Chaurasiya, T V S Subrahmanyam and Somiran Mandal for their dedicated technical assistance.

Appendix A. Supporting information

Supplementary data associated with this article can be found in the online version at doi:10.1016/j.physa.2025.130604.

Data availability

Data will be made available on request.

References

- [1] P. Richard, M. Nicodemi, R. Delannay, P. Ribiere, D. Bideau, Slow relaxation and compaction of granular systems, Nat. Mater. 4 (2) (2005) 121-128.
- [2] M.A. El-Emam, L. Zhou, W. Shi, C. Han, L. Bai, R. Agarwal, Theories and applications of CFD–DEM coupling approach for granular flow: a review, Arch. Comput. Methods Eng. (2021) 1–42.
- [3] J. Horabik, M. Molenda, Parameters and contact models for DEM simulations of agricultural granular materials: a review, Biosyst. Eng. 147 (2016) 206-225.
- [4] P.A. Cundall, O.D. Strack, A discrete numerical model for granular assemblies, Geotechnique 29 (1) (1979) 47-65.
- [5] Y. Duan, Z.G. Feng, A new kinetic theory model of granular flows that incorporates particle stiffness, Phys. Fluids 31 (1) (2019).
- [6] P. Wang, C. Arson, Energy distribution during the quasi-static confined comminution of granular materials, Acta Geotech. 13 (2018) 1075–1083.
- [7] Q. Sun, F. Jin, G. Wang, S. Song, G. Zhang, On granular elasticity, Sci. Rep. 5 (1) (2015) 9652.
- [8] LIGGGHTS(R)-PUBLIC Documentation, Version 3.X LIGGGHTS v3.X documentation. (n.d.). LIGGGHTS(R)-PUBLIC Documentation, Version 3.X &Mdash; LIGGGHTS v3.X Documentation. (https://www.cfdem.com/media/DEM/docu/Manual.html).
- [9] LAMMPS Molecular Dynamics Simulator. Available at: \(\https://www.lammps.org/index.html#gsc.tab=0\).
- [10] T. Li, Y. Peng, Z. Zhu, S. Zou, Z. Yin, Discrete element method simulations of the inter-particle contact parameters for the mono-sized iron ore particles, Materials 10 (5) (2017) 520.
- [11] J.R. Pillai, M.S.A. Bradley, R.J. Berry, Comparison between the angles of wall friction measured on an on-line wall friction tester and the Jenike wall friction tester, Powder Technol. 174 (1-2) (2007) 64–70.
- [12] T.T. Ng, Input parameters of discrete element methods, J. Eng. Mech. 132 (7) (2006) 723-729.
- [13] T. Foroutan, A.A. Mirghasemi, CFD-DEM model to assess stress-induced anisotropy in undrained granular material, Comput. Geotech. 119 (2020) 103318.
- [14] J. Schwedes, D. Schulze, Measurement of flow properties of bulk solids, Powder Technol. 61 (1) (1990) 59–68.
- [15] C. Li, T. Honeyands, D. O'Dea, R. Moreno-Atanasio, The angle of repose and size segregation of iron ore granules: DEM analysis and experimental investigation, Powder Technol. 320 (2017) 257–272.
- [16] R. Kumar, P.K. Jha, R. Kishore, R.K. Singh, T.V.S. Subrahmanyam, S.K. Chaurasiya, K.K. Sahu, Analysing the flow of wet iron ore in an industrial transfer chute using discrete element method, Miner. Process. Extr. Metall. 133 (4) (2024) 131–146.
- [17] D. Wang, M. Servin, T. Berglund, K.O. Mickelsson, S. Rönnbäck, Parametrization and validation of a nonsmooth discrete element method for simulating flows of iron ore green pellets, Powder Technol. 283 (2015) 475–487.
- [18] NMDC Ltd., India. (https://www.nmdc.co.in/), 2023 (Accessed 17 March 2023).
- [19] B. Yan, R.A. Regueiro, S. Sture, Three-dimensional ellipsoidal discrete element modeling of granular materials and its coupling with finite element facets, Eng. Comput. 27 (4) (2010) 519–550.
- [20] J. Ai, J.F. Chen, J.M. Rotter, J.Y. Ooi, Assessment of rolling resistance models in discrete element simulations, Powder Technol. 206 (3) (2011) 269–282.
- [21] C. Thornton, K.K. Yin, M.J. Adams, Numerical simulation of the impact fracture and fragmentation of agglomerates, J. Phys. D: Appl. Phys. 29 (2) (1996) 424.
- [22] K.E. Daniels, J.E. Kollmer, J.G. Puckett, Photoelastic force measurements in granular materials. Rev. Sci. Instrum. 88 (5) (2017).
- [23] R. Kishore, S. Das, Z. Nussinov, K.K. Sahu, Kinetic instability, symmetry breaking and role of geometric constraints on the upper bounds of disorder in two dimensional packings, Sci. Rep. 6 (1) (2016) 26968.
- [24] Y. Demirel, Nonequilibrium Thermodynamics: Transport and Rate Processes in Physical, Chemical and Biological Systems, Newnes, 2013.